JOURNAL OF MATERIALS SCIENCE 29 (1994) 554–561

Interfacial debonding and fibre pull-out stresses

Part IV *Influence of interface layer on the stress transfer*

JANG-KYO KIM*, SEHVOOM LU, YIU-WING MAI
Centre for Advanced Materials Technology, Department of Mechanical Engineering, University of Sydney, Sydney New South Wales 2006, Australia

The stress field arising in the fibre pull-out test is analysed by means of the finite element method. A focus has been placed on the roles of the compliant interlayer present between fibre and matrix for stress distributions in the constituents and debond process at the interface regions. In a parametric study on a carbon fibre–epoxy matrix composite, elastic properties and thickness of the interlayer were varied, and the results compared with those for composites without interlayers. The practical implications of the findings are critically discussed.

1. Introduction

A phenomenon of major importance in fibre composite technology for applications in engineering construction of load-bearing primary structures is the understanding of the stress transfer between fibre and matrix across the interface, particularly in the neighbourhood of a fibre break and matrix crack. The mechanical properties and chemical/morphological nature at the fibre–matrix interface region are key parameters controlling the structural/mechanical performance of fibre-reinforced composites. There is now considerable evidence to demonstrate the marked influences of interfaces on fracture toughness, strength and modulus in various failure modes and loading configuration [1, 2]. In the light of invaluable experiences and acquired knowledge based on the extensive experimental and theoretical investigations in the past three decades, the interface properties are becoming gradually accepted as design and/or process variables to be modified for desired effects in particular end applications of given combinations of fibre and matrix materials [3]. Many potential solutions for improving mechanical properties, fracture toughness and damage tolerance in particular, have been proposed for inherently brittle polymer matrix composites without sacrificing other important properties. Among the techniques devised for high fracture resistance, one of the most popular and effective methods is the application of an organic coating on to the fibre surface. It is well known that the fracture toughness of a composite is not simply the sum of the weighted contributions by the constituents of the composite, but is governed more importantly by the extent of energy absorption processes through various toughening mechanisms which are associated with interface fractures depending primarily on the nature of bonding at the fibre–matrix interface.

2. Background

2.1. Effects of interfacial coating

In our previous study [4] on unidirectional carbon fibre- and Kevlar fibre–epoxy matrix composites (CFRPs and KFRPs), the polyvinyl alcohol (PVAL) coating applied to the fibres before being incorporated into a matrix material has been shown to enhance the transverse fracture toughness of these composites by a remarkable 100% depending on the test temperature. This beneficial effect did not cause much reduction in flexural strength and fracture resistance of the composites against mode I and mode II interlaminar fractures [4, 5]. The major results of mechanical properties are summarized in Table I. The principal effect of fibre coating is to modify the fracture behaviour by altering the mechanisms of bond, stress states and other thermo-mechanical properties at the fibre–matrix interface region which, in turn, determine the energy absorption capability of the composites. To explain the roles of the thermoplastic coating which forms a discrete layer between fibre and matrix, three concepts of engineered interfaces have been put forward which include the weak interface-bond layer, the microductile/compliant layer and the compensating layer [6]. The weak bond layer promotes interfacial debonding and subsequent frictional fibre pull-out which gives rise to large contributions to the total composite fracture toughness. To achieve maximum benefits of high transverse fracture toughness arising from these failure mechanisms, a coating layer has to provide a sufficiently high frictional bonding while maintaining a weak (chemical) bonding at the inter-

* *Present address:* Department of Engineering, Faculty of Engineering and Information Technology, Australian National University, Canberra, ACT 0200, Australia.

0022–2461

TABLE I Mechanical properties of CFRPs and KFRPs with and without PVAL coating

Fibres	Transverse fracture toughness ($kJ\,m^{-2}$)	Flexural strength (MPa)	Interlaminar shear strength (MPa)	Interlaminar fracture toughness ($MPa\,m^{1/2}$)
Carbon				
uncoated	50.3	683	58.9	5.3
PVAL coated	98.7	758	50.5	5.1
Kevlar				
uncoated	139	518	42.6	–
PVAL coated	187	522	25.4	–

face. Morphological and chemical analyses of the composite fracture surfaces and fibre–matrix interfaces based on scanning electron microscopy and X-ray photoelectron spectroscopy confirm the weak interface bond due to the presence of the fibre coating [7]. Another beneficial effect of a weak interface bond in connection with the microductile/compliant layer concept is the crack-tip blunting and crack arrest/bifurcation which encourage further debonding and/or delamination along the fibre direction. The microductile/compliant layer reduces the local stress concentration by enabling the fibres to distribute more evenly the local stresses at the fracture process zone, particularly near the crack tip. This concept is best utilized when combined with the compensating layer which has a high coefficient of thermal expansion (CTE), and therefore the compressive stresses generated by the shrinkage of the stiff matrix material around the fibre upon cooling from the process temperature can be effectively balanced by the greater shrinkage of the compliant coating layer. The most important interlayer parameters for reducing the in-plane residual stresses are CTE, Young's modulus and thickness [8]. The latter two parameters were chosen to study their effects in the present finite element (FE) analysis discussed below.

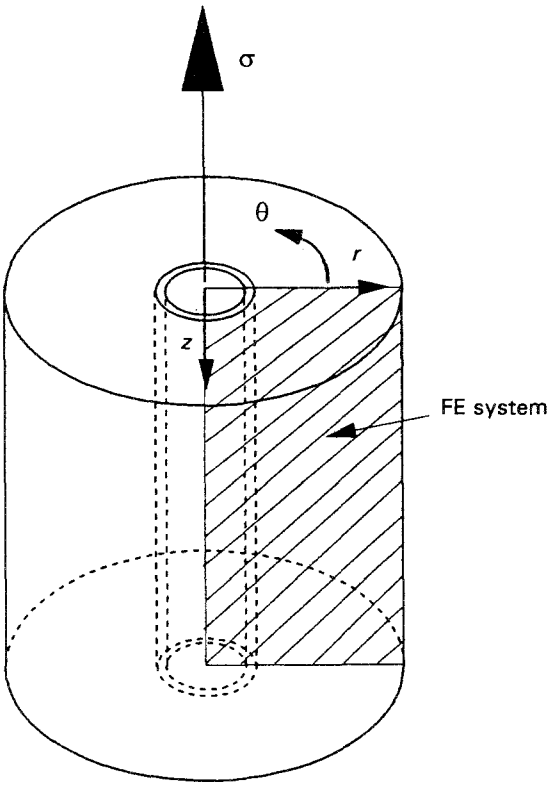

Figure 1 Schematic illustration of the pull-out test of the single-fibre composite with a coating layer.

2.2. Fibre pull-out test

The importance of interface properties in composite technology has directed significant research interests in recent years in both experimental and micromechanical/numerical characterization of the interface. Several experimental techniques have been developed to characterize the interface properties which include the fibre pull-out test, fibre fragmentation test and fibre push-out (or indentation) test. These single-fibre composite tests have been increasingly recognized as a useful tool to study the mechanical interactions near the interface, though there is a rather unrealistic stress state in the constituents due to the surrounding homogeneous matrix material instead of a fibre-reinforced material. The fibre pull-out test, in particular, is one of the most popular and reliable which is the subject of the present study (Fig. 1). In the theoretical analysis of fibre pull-out test, the condition of debonding at the fibre–matrix interface has been defined by two distinct approaches: the shear strength criterion and the fracture mechanics approach (or the critical energy release rate criterion). In the shear strength-based approach which has been adopted in the early work of Cox [9], Greszczuk [10] and many recent researchers, interfacial debonding occurs when the maximum interface shear stress reaches the interfacial bond strength, τ_b. In the energy-based approach, extension of a debond crack requires the energy release rate to reach a critical value, the interfacial fracture toughness, G_{ic}. The latter concept has been successfully used to develop an improved analytical model recently by the authors [11], which clearly shows that the debond stress during the progressive debond process consists of the frictionless debond stress and the friction stress components. These two stress components are a function of the interface properties, respectively, at the bonded region (e.g. interfacial fracture toughness, G_{ic}) and at the debonded region (e.g. coefficient of friction, μ, and residual clamping stress, q_o). Also identified are the instability conditions during the progressive debond process [12] which has practical significance in controlling the fracture behaviour of composites containing short fibres. The theory compares favourably with the experimental data for several different composite sys-

tems including carbon fibre–epoxy matrix, steel fibre–epoxy matrix and SiC fibre–glass matrix composites.

In addition to the analytical micromechanics models of the fibre pull-out test discussed above, many investigators have performed numerical analyses of single-fibre composite tests of various loading geometry, using especially the finite elements (FE) methods. These include fibre pull-out test [13, 14], microdebond test [15, 16] which is a modified version of fibre pull-out test, fibre fragmentation test [16, 17] where a short fibre is embedded completely inside a matrix material which is subjected to uniaxial tension, and fibre push-out (or indentation) test [18]. Major concerns of these studies were the influences of the dimensions and shape of the specimen, loading methods, material properties on the stress distributions in the composite constituents which are occasionally compared with the results obtained from other micromechanics and photoelastic analyses. Relatively little work has been reported of the FE analysis on single-fibre composite models containing coatings or interlayers between fibre and matrix. Daabin *et al.* [19] analysed a fibre fragmentation model where the effects of properties of composite constituents are studied on the interface shear stress before interface debonding. Based on the comparisons between the maximum stresses, they proposed that a debond crack is likely to initiate at the fibre/coating interface rather than at the coating/matrix interface. Tsai *et al.* [20], based on a FE study of the fibre push-out test, have found significantly lower shear stress concentrations near the fibre entry when there is a compliant interlayer at the fibre–matrix interface. The maximum shear stress is shown to occur at approximately 80% of the fibre radius below the fibre entry (or matrix surface).

In the present study, as an extension of the previous work on micromechanics analyses of fibre pull-out test [11, 12], a FE method is used to investigate further the effects of the compliant fibre coating on the stress transfer between the fibre and matrix across the interface. In a parametric study the stress distributions in the constituents and at the fibre/coating and coating/matrix interfaces are specifically characterized for varying elastic modulus and thickness of the coating before and during the debond process.

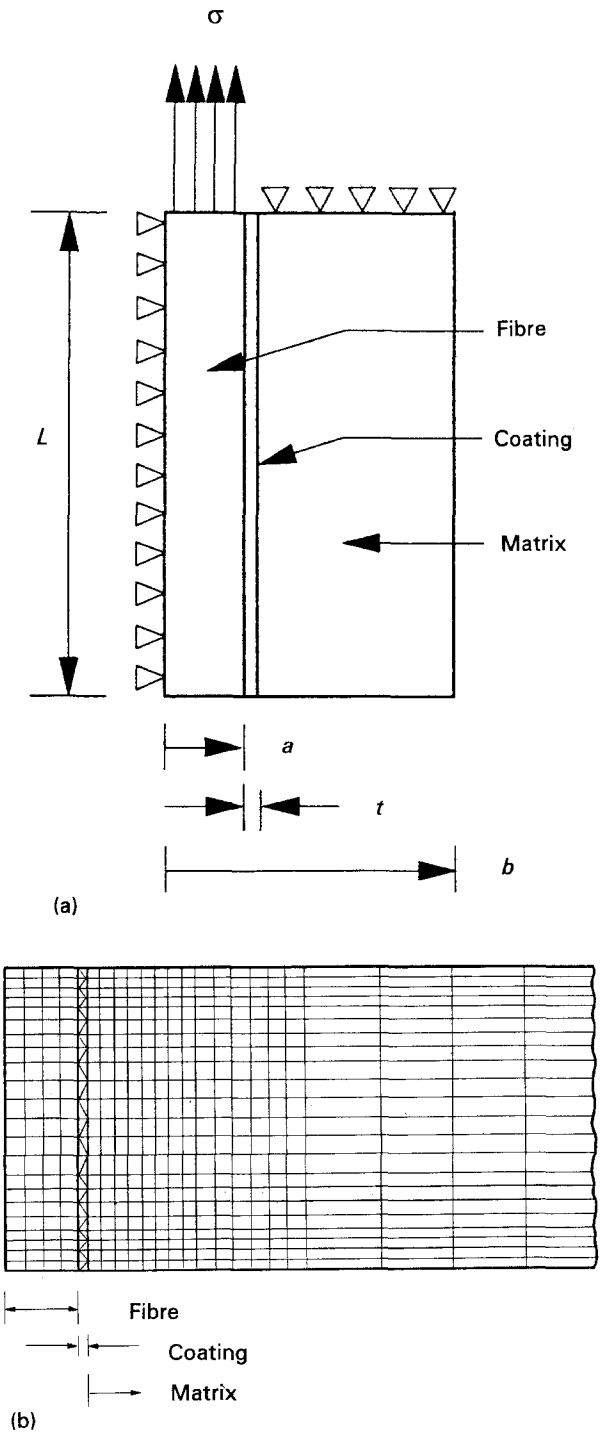

Figure 2 Schematic illustrations of (a) the finite element model for the fibre pull-out test and (b) the finite element mesh.

3. Finite element (FE) model

Following previous micromechanics analyses [11, 12], a simple shear-lag model is considered as shown in Figs 1 and 2(a) where a fibre (of radius a) with a coating layer (of thickness t) is embedded at the centre of a coaxial cylindrical shell of matrix (of an outer radius b). A uniformly distributed external stress, σ, is applied to the free end of the fibre (with embedded length L). A set of cylindrical coordinates (r, θ, z) is chosen so that the z-axis of the fibre corresponds to the longitudinal direction of the fibre from top to bottom. Therefore, the axisymmetric loading geometry of the fibre pull-out allows development of a two-dimensional model using the FE program "Strand 6". The geometry of the model, the loading method and the boundary conditions are selected to represent those of the actual experimental technique. To ensure sufficient accuracy of the results while maintaining a reasonable time required for computation, a mesh has been created such that the total number of elements are 726, with 22 and 33 elements in the axial and radial directions, respectively (Fig. 2b). Isometric eight-node quadrilateral elements are used for the fibre and matrix, while a layer of six-node triangular elements are used for the coating. Boundary conditions are imposed such that the matrix top (at $z = 0$) and the coaxial axis (at $r = 0$) are fixed. The bottom and cylindrical surface of the matrix are set to free, and hence the global default freedom is set to allow displacements in the z- and r-directions.

TABLE II Mechanical properties of composite constituents

Constituents	Elastic modulus (GPa)	Poisson's ratio
Carbon fibre	$E_f = 230$	$\nu_f = 0.2$
PVAL coating	E_c = varied	$\nu_c = 0.35$
Epoxy matrix	$E_m = 3.0$	$\nu_m = 0.4$

A carbon fibre of embedded length $L = 200$ μm and radius $a = 50$ μm with an epoxy matrix of radius $b = 500$ μm is considered throughout the present study. The fibre, coating and matrix materials are assumed isotropic and perfectly elastic. The coating layer between the fibre and matrix is regarded as a distinctive region with its own mechanical/physical characteristics and perfect bonding to the fibre surface and the matrix. The present analysis examines the stress states in the constituents both before and after a debond crack initiates at the interface region. For elastic stress transfer before debond initiation, a constant external stress $\sigma = 10$ MPa is applied. During the debond process, the maximum interface shear stress is closely monitored as the external stress is increased for a given debond length so that the external stress is taken as the instantaneous partial debond stress, σ_d^p, when the former stress reaches the interface bond strength, τ_b, based on the shear-strength criterion. Because no friction is assumed for the debonded region in the present study, σ_d^p represents here the frictionless debond stress. $\tau_b = 72.7$ MPa, which is measured from the fibre pull-out test of similar carbon fibre–epoxy matrix composites [12], is used for the composite without coating, and approximately half the value (i.e. $\tau_b = 36.4$ MPa) is taken for the coated composites. In a broad-based study, Young's modulus and thickness of the coating are varied. Other mechanical properties used for the calculations are given in Table II. All stress values herein are normalized with the external stress unless otherwise specified. Negative signs for the matrix axial stress and the interface shear stress are omitted for simplicity.

4. Stress distributions in the composite constituents

4.1. Elastic stress transfer

The fibre stress distributions in the axial direction shown in Fig. 3 are taken from the centre of the fibre at $r = 0$ for the composite with interfacial coating of thickness $t = 5$ μm. The fibre axial stress, σ^{zz}, decreases from a maximum at the fibre entry towards zero at the fibre end. The radial and tangential stresses, σ^{rr} and $\sigma^{\theta\theta}$, also decrease from a maximum at the fibre entry and become almost negligible for the middle half of the fibre length. These stresses are compressive near the embedded end of the fibre. The fibre is free of shear stress, τ^{rz}, over almost the whole embedded fibre length except at the fibre entry. As a whole, a large stress concentration is generated near the fibre entry which is transferred to the matrix across the interface.

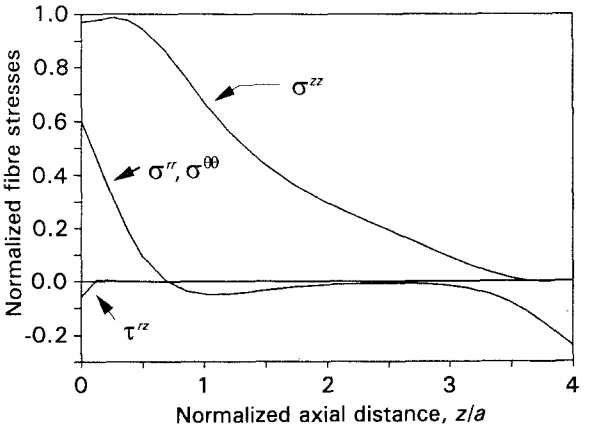

Figure 3 Stress distributions in the fibre for coating thickness $t = 5$ μm and Young's modulus ratio of the coating to the matrix $E_c/E_m = 0.5$.

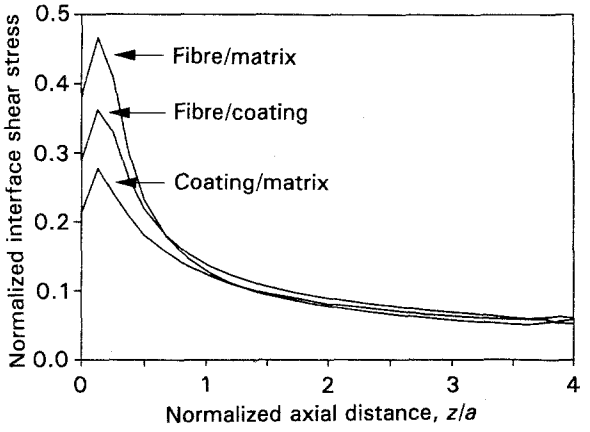

Figure 4 Interface shear stress distributions for the composites with and without a coating layer ($t = 5$ μm and $E_c/E_m = 0.5$)

The interface shear stresses shown in Fig. 4 have several points of interest. First of all, it is clearly demonstrated that there is a large stress concentration near the fibre entry. The maximum stress always occurs at a short distance (approximately 4% of the embedded fibre length, or equivalently 16% of the fibre radius) away from the fibre entry for all three interfaces studied. This maximum stress is invariably followed by a parabolic decay towards almost a constant value over the bottom half of the embedded fibre length. The above general trend of maximum interfacial shear stress agrees well with previous FE analyses of the single-fibre composite models [16, 18–20], but is in sharp contrast to the prediction of a maximum shear stress right at the fibre entry (or at the matrix surface) based on a micromechanics model [11] and other FE analyses [14, 15, 17]. Apart from the complication associated with the stress singularity at the boundary or at the crack tip, the exact location of the peak stress concentration seems to depend largely on the FE software as well as the fineness of the element mesh. Secondly, the interface shear stresses for the composite without the coating are substantially higher than those with coating at the region of stress concentration near the fibre entry. This confirms that the compliant coating acts as a stress-relief medium

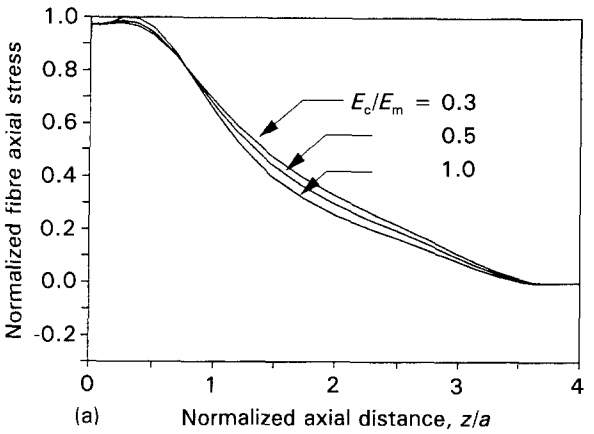

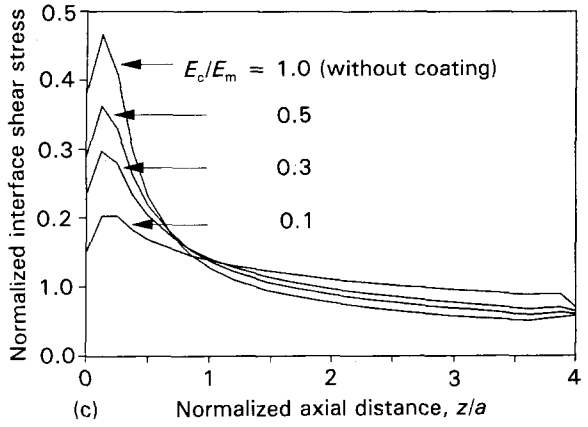

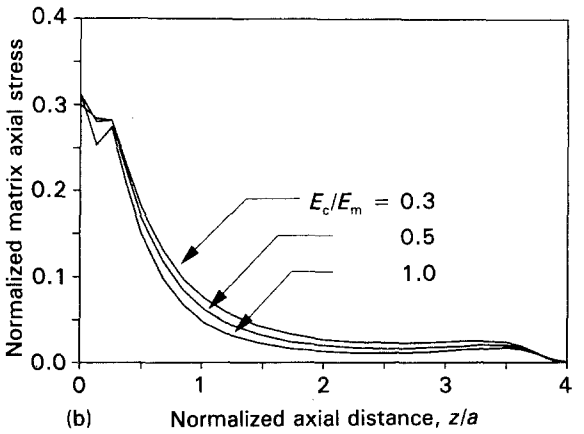

Figure 5 (a) Fibre axial stress, (b) matrix axial stress, and (c) shear stress at the fibre/coating interface for different ratio of Young's modulus of the coating to the matrix, E_c/E_m (t = 5 μm).

reducing the stress concentration [6]. Thirdly, in the composite with a fibre coating, the shear stress is higher at the fibre/coating interface than at the coating/matrix interface. This has an important practical implication in that debonding would initiate at the fibre/coating interface in preference to the coating/matrix interface (if assuming that the bond strength or interface fracture toughness at these two interfaces are identical). A similar conclusion has been suggested recently [19] based on a FE analysis of the fibre fragmentation test for a SiC fibre–titanium matrix composite.

The fibre axial stress, matrix axial stress and shear stress at the fibre/coating interface are shown in Fig. 5 where in the Young's modulus ratio of the coating to the matrix, E_c/E_m, is varied from 0.1–1. The elastic modulus of the coating has little effect on the stress distributions both in the fibre and matrix axial directions. This is expected, due probably to the low volume fraction of the coating compared with the other composite constituents (i.e. coating thickness t = 5 μm, compared with the radii of the fibre and matrix of 50 and 500 μm, respectively). A lower E_c/E_m resulted in only a slightly higher stress distribution with a lower stress gradient in the middle of the embedded fibre. In sharp contrast, Young's modulus ratio is very much influential in controlling the interface shear stress. The maximum interface shear stress and the stress gradient along the fibre axis drop sharply as E_c/E_m is reduced. When E_c/E_m = 0.1 (i.e. for a very compliant coating) the interface shear stress becomes almost constant over the whole embedded fibre length, with almost completely diminished stress concentration near the fibre entry. This pronounced effect of Young's modulus ratio is summarized in a plot of maximum shear stresses versus E_c/E_m, in Fig. 6, which indicates an approximately linear dependence between these two parameters both at the fibre/coating and coating/matrix interfaces. This result further suggests that the more compliant is the coating layer, the more reduction there is in stress concentration. Again, the maximum values obtained at the fibre/coating interface are shown always to be higher than those at the coating/matrix interface for a given E_c/E_m value, which is consistent with the finding from Fig. 4.

The effects of coating thickness on the stress distributions along the fibre direction and the maximum values for the interface shear stresses are illustrated in Figs 7 and 8, respectively. As expected, increasing the thickness of the compliant coating reduces both the stress concentration and the stress gradient along the fibre axis. The maximum shear stresses obtained both at the fibre/coating and coating/matrix interfaces decrease approximately linearly with increasing coating thickness when the coating is thinner than about 8 μm, which is followed by almost a constant value independent of the coating thickness when the coating is sufficiently thick. This observation is particularly relevant to practical design of composite materials in that

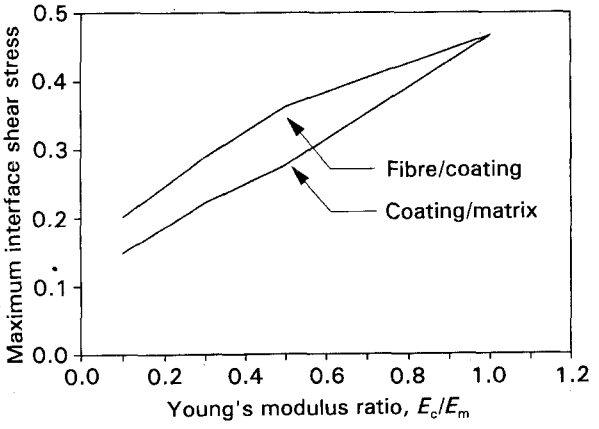

Figure 6 Maximum interface shear stresses as a function of Young's modulus ratio, E_c/E_m (t = 5 μm).

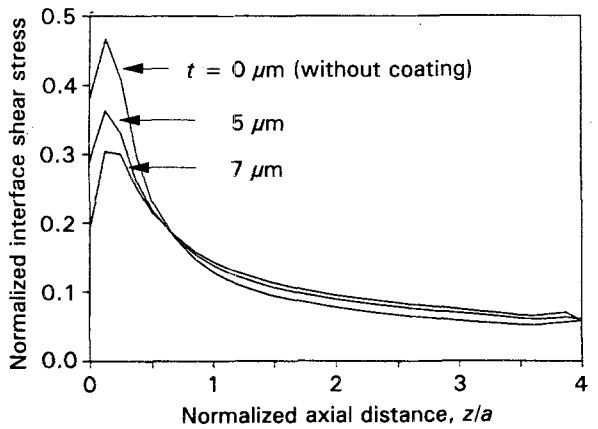

Figure 7 Interface shear stress distributions for the composites with and without coating (t = 5 μm and E_c/E_m = 0.5).

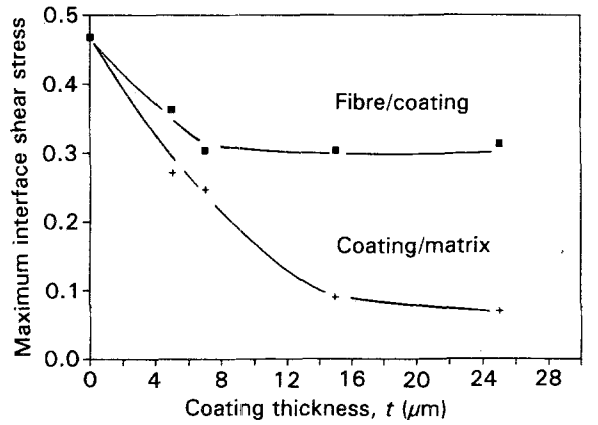

Figure 8 Maximum interface shear stresses as a function of coating thickness, t (E_c/E_m = 0.5).

there is an optimum coating thickness for given elastic properties of the constituents which imparts the lowest stress concentration at the interface while minimizing possible reduction in strength and stiffness due to the presence of the compliant interfacial coating. The optimum coating thickness determined based on the lowest maximum shear stresses both at these interfaces is approximately 15 μm when E_c/E_m = 0.5 and other properties of the fibre and matrix are as given in Table II. It is expected that this value is further reduced if a more compliant coating material is employed.

4.2. Stress distributions during the debond process

The general pattern of the stress distributions in the composite constituents versus axial distance during the debond process shown in Fig. 9 are similar to those before debond initiation, except at the debonded region (for the range of axial distance $0 \leqslant z/a \leqslant 1.2$) where the stresses are almost constant, within the accuracy of calculation, due to the assumed zero friction. However, the influence of Young's modulus ratio on the axial stress distributions in the fibre and matrix is far more significant during the debond process than before debond initiation (compare Figs 9 and 5). This result seems to be in part associated with the significantly higher external stress for debond crack propagation. Similar stress distributions versus axial distance are shown in Fig. 10 for different coating thicknesses. It is worth noting that a small increase in coating thickness (from t = 5 μm to 7 μm) does not alter at all the stress state in the constituents. However, the presence of a compliant coating of this range of thickness reduces significantly all three stress components compared to those for composites without a coating layer. A constant value of interface shear strength, τ_b = 36.4 MPa, chosen for the composite with fibre coating irrespective of the coating thickness, is responsible for this result. Therefore, a larger difference in stress distributions would be expected during

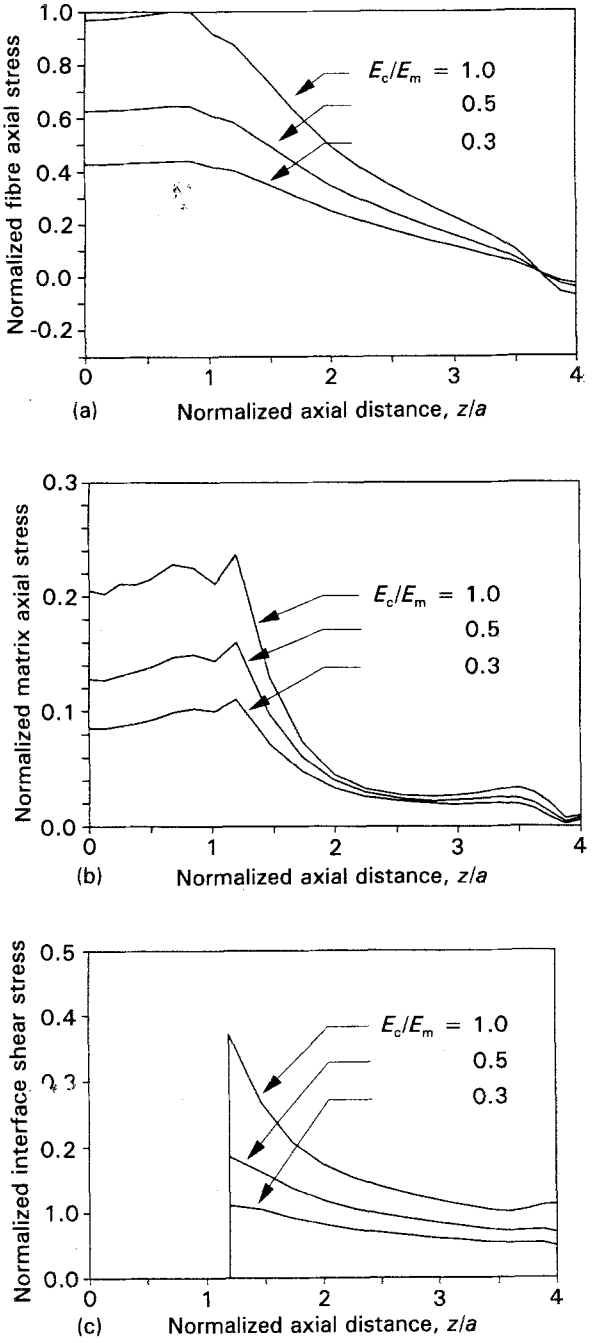

Figure 9 (a) Fibre axial stress, (b) matrix axial stress, and (c) shear stress at the fibre/coating interface for different ratio of Young's modulus of the coating to the matrix, E_c/E_m (t = 5 μm and debond length l/a = 1.2).

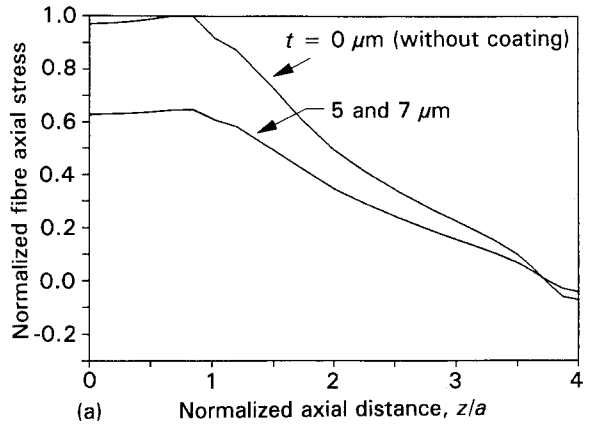

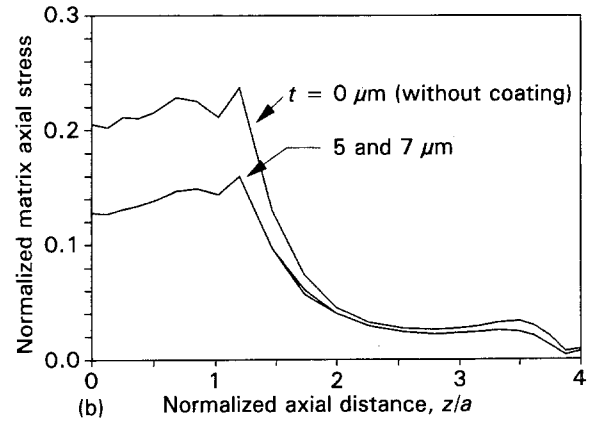

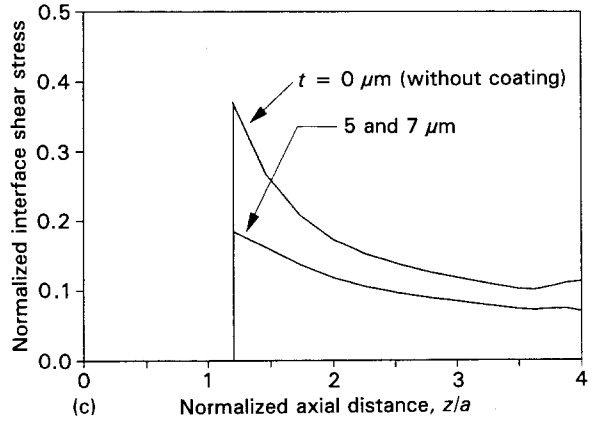

Figure 10 (a) Fibre axial stress, (b) matrix axial stress, and (c) shear stress at the fibre/coating interface for different coating thickness, t ($E_c/E_m = 0.5$ and debond length $l/a = 1.2$).

the debond process if the interface bond strength were varied depending on the coating thickness.

The partial debond stress, σ_d^p, obtained during the debond process (normalized with the maximum value for the composite without the coating layer) is always greater for the uncoated composite with a strong interface bond than the composite with a coating layer for the whole debond process of a given embedded fibre length (Fig. 11). The curve for the composite without coating is comparable to the prediction calculated based on a micromechanics analysis [11]. The gradual increase in σ_d^p to a maximum value over a small debond length predicted in the present FE analysis appears to be closely related to the high stress

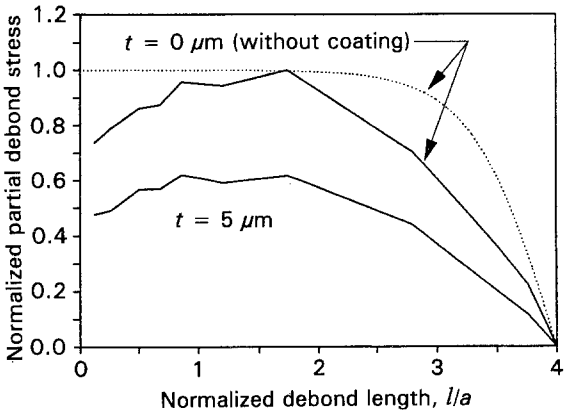

Figure 11 Partial debond stress, σ_d^p, as a function of debond length, l/a, for composites with and without coating layer: (– – –) prediction [11].

concentration caused by the restrained matrix top condition which puts the matrix material at the interface region under a high compressive stress, near the matrix surface or the crack tip in particular. This results in a low external stress required for debond initiation. Sharp peaks of the matrix axial stress at the boundary between the bonded and debonded regions (i.e. at $z/a = 1.2$ in Figs 9b and 10b) partly support this hypothesis. As the debond length increases, the influence of the concentration of this compressive stress diminishes. (For the micromechanics model [11] the matrix bottom was fixed.)

5. Conclusion

A finite element method is used to study the stress transfer in the composite constituents for the single-fibre pull-out model both before and after a debond crack has initiated at the fibre–matrix interface. The compliant coating layer which forms a discrete layer between fibre and matrix significantly reduces the stress concentration occurring particularly near the fibre entry. Within the composite containing such a coating layer, the interface shear stress is always higher at the fibre/coating interface than at the coating/matrix interface, an indication of debond initiation at the former interface in preference to the latter interface. Major parameters which control the effectiveness of the interlayer include Young's modulus ratio of the coating to the matrix and coating thickness. All these findings are basically in line with the residual stresses [6] resulting from matrix shrinkage upon cooling from the process temperature which are predicted based on a thermo-mechanical analysis of the fibre/coating/matrix three cylinder model.

Within the limitation of available data, the present paper further studies the roles of the compliant fibre coating in controlling the stress transfer across the fibre–matrix interface and debond behaviour in the fibre pull-out model. In this parametric study, virtually no attempt has been made to compare the present FE model with relevant experimental results or other theoretical models developed by means of micromechanics/numerical analyses. This is partly due to the lack of such studies hitherto, particularly for those

composite models containing compliant interfacial coatings, which will be the subject of forthcoming publications.

Acknowledgements

The authors thank the Australian Research Council (ARC) for the continuing support of this project, and J.K.K. is particularly grateful for the Australian Post doctoral Research Fellowship awarded by the ARC when part of the work was performed at the University of Sydney. Part of this paper was presented at the International Conference ACMSM-13 (Wollongong, Australia, July 1993).

References

1. J. K. KIM and Y. W. MAI, *Compos. Sci. Technol.* **41** (1991) 333.
2. L. T. DRZAL and M. MADHUKAR, *J. Mater. Sci.* **28** (1993) 569.
3. J. K. KIM and Y. W. MAI, in "Structure and Properties of Fibre Composites", Materials Science and Technology, Series Vol. 13, edited by T. W. Chou (VCH, Weinheim, Germany, (1993) Ch. 6 pp. 239–289.
4. *Idem, J. Mater. Sci.* **26** (1991) 4072.
5. X. Z. HU and Y. W. MAI, *Compos. Sci. Technol.* **46** (1993) 147.
6. J. K. KIM and Y. W. MAI, "Fracture Mechanics: 25th Volume", *ASTM STP* 1220, edited by F. Erdogan and R. J. Hartranft (ASTM, Philadelphia, PA, 1994) in press.
7. J. K. KIM, Y. W. MAI and B. J. KENNEDY, *J. Mater. Sci.* **27** (1992) 6811.
8. S. M. ARNOLD, V. K. ARYA and M. E. MELIS, *J. Compos. Mater.* **26** (1992) 1287.
9. H. L. COX, *Br. J. Appl. Phys.* **3** (1952) 72.
10. L. B. GRESZCZUK, "Interfaces in Composites", *ASTM STP* 452 (ASTM, Philadelphia, PA, 1969) pp. 42–58.
11. L. M. ZHOU, J. K. KIM and Y. W. MAI, *J. Mater. Sci.* **27** (1992) 3155.
12. J. K. KIM, C. BAILLIE and Y. W. MAI, *ibid.* **27** (1992) 3143.
13. C. ATKINSON, J. AVILA, E. BETZ and R. E. SMELSER, *J. Mech. Phys. Solids* **30** (1982) 97.
14. Ch. MAROTZKE, *Compos. Interfaces* **1** (1993) 153.
15. H. F. WU and C. M. CLAYPOOL, *J. Mater. Sci. Lett.* **10** (1991) 260.
16. P. H. HERRERA-FRANCO and L. T. DRZAL, *Composites* **23** (1992) 2.
17. Y. TERMONIA, *J. Mater. Sci.* **22** (1987) 504.
18. M. N. KALLAS, D. A. KOSS, H. T. HAHN and J. R. HEKKMANN, *J. Mater. Sci.* **27** (1992) 3821.
19. A. DAABIN, A. J. GAMBLE and N. D. SUMNER, *Composites* **23** (1992) 210.
20. H. C. TSAI, A. M. AROCHO and L. W. GAUSE, *Mater. Sci. Eng.* **A126** (1990) 295.

Received 30 June
and accepted 24 August 1993